MAFF — Munich Accelerator for Fission Fragments

D. Habs, R. Krücken, M. Groß, T. Faestermann, W. Assmann, L. Beck, H. Bongers, W. Carli, S. Emhofer, R. Großmann, P. Hartung, S. Heinz, P. Jüttner [a], O. Kester, H.J. Maier, P. Maier-Komor, F. Ospald, M. Pasini, K. Rudolph, M. Schumann, J. Szerypo, P.G. Thirolf, F. Tralmer [a], and E. Zech
[a] Forschungsreaktor München II, Garching

The **M**unich **A**ccelerator for **F**ission **F**ragments (MAFF), a reactor-based Radioactive Ion Beam (RIB) facility, is being planned and set-up at the FRM-II mainly by the groups for experimental nuclear physics at the LMU (Prof. Habs) and the TUM (Prof. Krücken).

The goal of this installation is the production of very intense beams of neutron-rich isotopes that will be available for a broad range of nuclear physics experiments as well as applied physics and nuclear medicine. In a first step the beam will have an energy of 30 keV (low-energy beam). In a second step also a high-energy beamline will be set up where the ions are post-accelerated to energies adjustable in the range 3.7–5.9 MeV/u. An overview of the project can be found, e. g. in [1,2]. Here we will summarize mainly the progress within the last year.

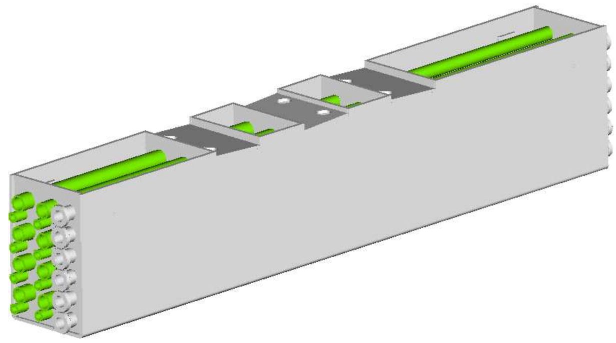

Fig. 1: The feedthrough-plug between neutron guide hall and neutron guide tunnel

1. Authorization procedure

MAFF is at present still in the design and planning stage, as a dedicated authorization procedure will be necessary to set up and run the instrument. This procedure will commence only after FRM-II has received its final authorization.

Apart from preparing documents, the safety barrier concept of MAFF with respect to loss of pool water and release of radioactivity has been revised and mostly agreed by TÜV Süd.

2. Preparatory work

2.1 Cryosystem

The cryosystem being an essential part for running MAFF already in the first stage, the compressor will be placed at the UTA building. The arrangement of pipelines has been planned by KAM (Kraftanlagen Anlagenbau München).

2.2 The feedthrough-plug to the neutron guide tunnel

The neutron guide tunnel of the FRM-II will house the mechanics to move the target trolley and to operate the ion source changer. As the operational reliability of these components is crucial for MAFF, a manually driven backup system is foreseen. Due to the high activity level in the tunnel, this system must be operated from outside, more precisely from the neutron guide casemate. There are openings in the wall that are up to now only used by the neutron guides and the remaining space will be filled with bricks very soon in order to fulfill radioprotection and security requirements. We will therefore place a special plug containing several feedthroughs alongside a neutron guide in the wall opening. The feedthroughs will contain shafts to operate the trolley in case of failure of the electric drives along the beamline in the neutron guide tunnel as well as gas pipes to connect the cryopumps at the beamline to the compressors which will be placed in the casemate.

2.3 Setup for beamline alignment test

A setup was designed in order to allow for a check of the alignment of the already installed beamline SR6 at the FRM-II prior to any other interior installations. For this purpose cross hairs will be moved along the beamline while optically monitoring its alignment from the outside. In order to allow for a self-centering of the cross hairs while moving through the potentially imperfectly round beam tube, a commercial (polypropylene/polyamide) brush was chosen as carrier medium of the cross hairs. The brush will be guided by a (6 m) long aluminum tube through the wide-diameter regions of the beamline SR-6 to allow for a smooth entering into the central part of the beamline with the smallest inner diameter of 155 mm. A (ca. 8 m) rod will be used to move the brush from the outside. The guiding tube with brush and rod will be mounted onto a support structure which itself can be moved on a wheel system on the floor (aligned parallel to the beam axis) for inserting the tube into the SR-6 beamline. Before installing this setup at the FRM-II, tests are foreseen at the MLL, were a test beamline exists that geometrically duplicates the situation of the SR-6 beamline. The self-centering capability of the brush carrying the cross hairs will be tested as well as the possibility to move the whole system back and forth.

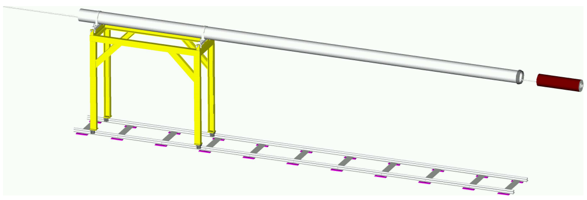

Fig. 2: Schematical view of the setup for testing the alignment monitoring system for the beamtube SR-6.

3. Development of components

3.1 The MAFF target ion source

The main part of the MAFF inpile structure is the MAFF target ion source [3]. As the ion beam intensity mainly depends on the speed and efficiency of the diffusion, effusion and extraction of the fission products, the target ion source in a high flux reactor environment is a crucial issue. The source construction should be as simple as possible to improve the reliability in the hostile environment and to facilitate the removal and disposal of the source (10 kCi activity after one reactor cycle of operation and 1 g U content). The source will be mounted on a supporting rod and remote-controlled placed at the point of maximum thermal neutron flux (about $1.5 \cdot 10^{14}$ n/cm^{2}s), at 60 cm distance to the reactor core inside the through-going zircaloy beam tube SR6. The source operation must be reliable and last for one reactor cycle. Therefore the source construction and some fundamental features have been examined with a source prototype. Several types of ion sources are required to cover the elements in the entire mass range. Beside the surface ionizer, a plasma ion source and a resonant laser ionisation source are planned.

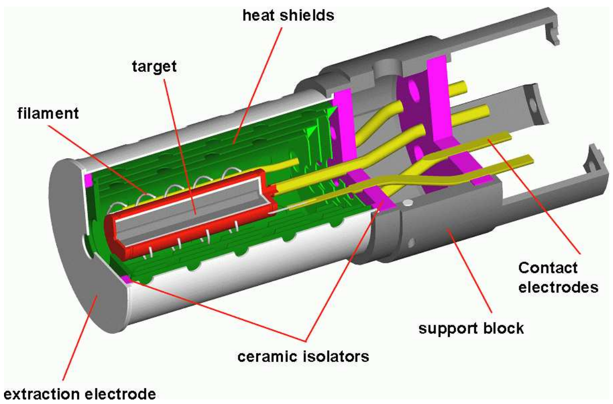

Fig. 3: Structure of the MAFF target-ion source prototype.

The most simplest type of ion source, which will be developed first, is the surface ionization source. This prototype is based on the ANUBIS source at the OSIRIS facility in Studsvik. Figure 3 shows the structure of the MAFF test source. The surface ionisation source provides high ionisation efficiencies of up to 100 % for alkaline metals. Some modifications have been made to the ANUBIS design in order to master the operational conditions. Much effort was spent on the development of appropriate uranium-loaded graphite targets. The target will be externally heated by low-tension electron bombardment from a tungsten filament and kept in a temperature range of 1500–2400° C, which provides rapid effusion of the fission products into the target channel. The target is embedded in a cylinder consisting of glassy carbon and a protective rhenium container with a 2 mm diameter orifice, where surface ionization takes place. The glassy carbon sheath prevents diffusion losses of U and of fission products across the target surface, while the Re container gives additional mechanical strength to the target assembly. Re has been chosen, because it is most inert against C and U at high temperatures, has a high melting point (3180° C) and is not affected significantly by the high neutron flux. Moreover, due to its distinct chemical inertness, the Re container provides protection against oxidation of the target in case of air-or water influx into the beamline.

Six different types of carbon have been investigated for their capability of incorporating U at a sufficient quantitity and a sufficiently homogeneous dispersion [4]. It was found, that the graphite type PG 100, manufactured by UCAR, is the most promising material for our purpose. A sample having the standard dimensions of 15 mm diameter and 60 mm length with a single-ended central channel of 5 mm diam. and 55 mm length can absorb 1.25 g of U while featuring an excellent homogeneous dispersion.

Four heat shields are required to confine the high target temperature of the prototype source. Three electric isolated inner shields, which are used as Wehnelt electrodes for beam formation and one outer shield, which is used as the extraction electrode. Although Re does not show optimum neutron capture properties, the two inner shields will be manufactured out of Re. Nb and Mo are no alternatives for these strongly temperature-stressed parts, because of their comparatively low melting points. W and Ta should be avoided as well, because of their long-term neutron-induced radioactivity. The two outer heat shields will be made from Mo in the real source. The filament is used for electron bombardement, which allows to fine adjust the target temperature in case of uranium load or to heat the target in case of pure graphite targets. In order to simplify the mechanical production of the prototype and to study the mechanical stability, the prototype has been made from materials which could be handled by our workshop. Thus the target cylinder was made from Ta and the heat shields from stainless steel. Welding of the Ta cylinder was performed by WIG-welding in a glovebox containing an Ar atmosphere with a content of 4 vpm O_2 and 0.1 vpm H_2O. This procedure is also suitable for welding of Re parts. The test source unit without heat shields is shown in figure 4. The purpose of the test source had been the test of the filament heating, the electron bombardement, temperature measurements at the source body and the heat shields, as well as the test of the beam formation.

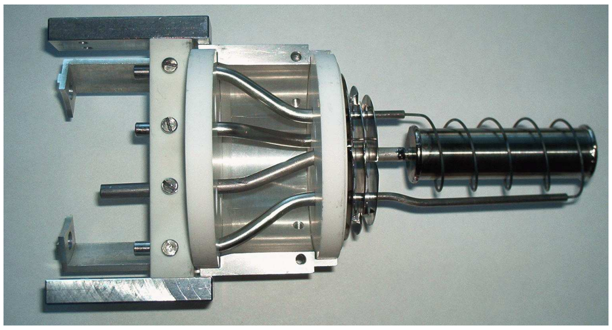

Fig. 4: Photograph of the test ion source unit without heat shields.

Several Tungsten filaments with different wire strengths have been tested [5]. As a result of the horizontal mounting of the source, a minimum wire strength of 0.75 mm is required. Wires with a smaller diameter will sag due to the high temperatures. Heating of the target by electron bombardment emitted from a hot filament was possible with beam currents in the aspired order of magnitude of 1 A. The temperature could be varied between 1100 and 1500° C. Temperature measurements have shown that the outer heat shield will reach 420° C and the support structure 160° C, for target temperatures of 1100° C. The power losses due to radiation and heat conductance has been measured in dependence on the filament temperature. Figure 5 shows the results for a filament of 1 mm thickness. The main contribution of non-radiative power losses is not the heat conduction but resistive loads between the vacuum feedthroughs and the connecting cables towards the source electrodes. For a prototype with materials for high temperatures, the cable contacts will be optimized with respect to conductivity.

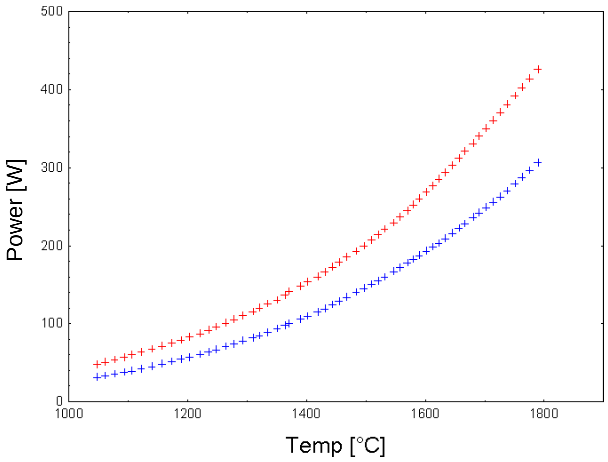

Fig. 5: Power dissipated due to radiation (lower curve) and total power dissipated in the filament.

At the ion source laboratory of the MLL, experiments on ion extraction from the prototype were performed The currents expected for the MAFF project are in the order of magnitude of 10 μA. Thus space charge effects must not be considered. Emittance measurements of the ion beam have been carried out. Transverse emittances between 14 and 25 π mm mrad have been measured, which did exceed the expected values from simulation calculations in the order of 10 π mm mrad. The reasons of this discrepancy are several components in the beam, which could be determined in mass spectra, and a larger ionizing surface than had been assumed in the calculations. The basic concept for the MAFF ion source could be confirmed but basic changes in the mechanical set-up will be required for better heat shielding, better mechanical stability and to avoid metallic vapor deposition on the insulators. These changes will be included in a prototype consisting of reactor suitable materials.

3.2 The vacuum system

The vacuum system of the low energy MAFF beam tube can be divided into three sections to ensure the required safety concept which must be approved by the authorities (TÜV). Experiences from CERN and Grenoble which led to the concept of the PIAFE proposal [9], [10]) were fully heeded. In the meantime, however, new developments of vacuum pumps allowed to modify the pumping philosophy (Fig. 6). In the PIAFE draft, turbomolecular pumps were planned as the main high vacuum pumps. This would have meant four main disadvantages:

1. The required redundancy can only hardly be fulfilled, because the reserve pumps should also run in the stand-by modus, otherwise their high-speed ball bearings might settle and the pump might not be started again.

2. A turbomolecular pump can only transport the gases to a forepump and from there into storage tanks, where the radioactive load (fission products) can decay. In this way even the short living fission products leave the well shielded area and require there spacious shielding for the decay tanks.

3. In case of a failure of a turbomolecular pump, repairing is not possible due to the radioactive inventory. The expensive pump would create voluminous radioactive waste.

4. Since the vacuum system will not be baked, the UHV region cannot be reached. Thus the dominant partial pressure (about 90 %) will be water vapor. For such light molecules turbomolecular pumps have a low pumping speed, whereas cryopumps with the same inlet flange offer a five times higher pumping speed for water vapor.

The huge amount of volatile, mostly short living radioactive fission products which enter the vacuum system can be trapped in a refrigerator cryopump. Since these cryopumps are mounted closely to the beam tube or to the radioactively contaminated vacuum vessels they can be housed in the same shielding cave. The capacity of such cryopumps is good for several reactor cycles of 52 days each. Thus the redundancy is not violated when e.g. a cryopump is filled during one reactor cycle and then waits for regeneration in stand-by mode for another two months.

For regeneration, the cryopump is switched off and is evacuated during warm-up via a forevacuum valve by means of a roughing pump down to 5 Pa. During regeneration the exhaust port of the roughing pump is connected to a decay tank which size is sufficient that discharge into the exhaust gas system of the reactor (KLA 70) should be necessary once a year only. The half-life of the longest living noble gas (^{133}Xe) is 5.25 d, thus it will have decayed by more than twenty orders of magnitude before being released in the environment. Solid fission products or solid daughters of volatile fission products might be bound as aerosols and thus can be transported to the exhaust system. In order to prevent this, a mechanical filter for grain sizes > 0.1 μm and an efficiency of 99.99 % is installed in front of the roughing pump of KLA 70. In principle it is not likely that solid fission products reach the filter element. Most are bound in the cryopumps.

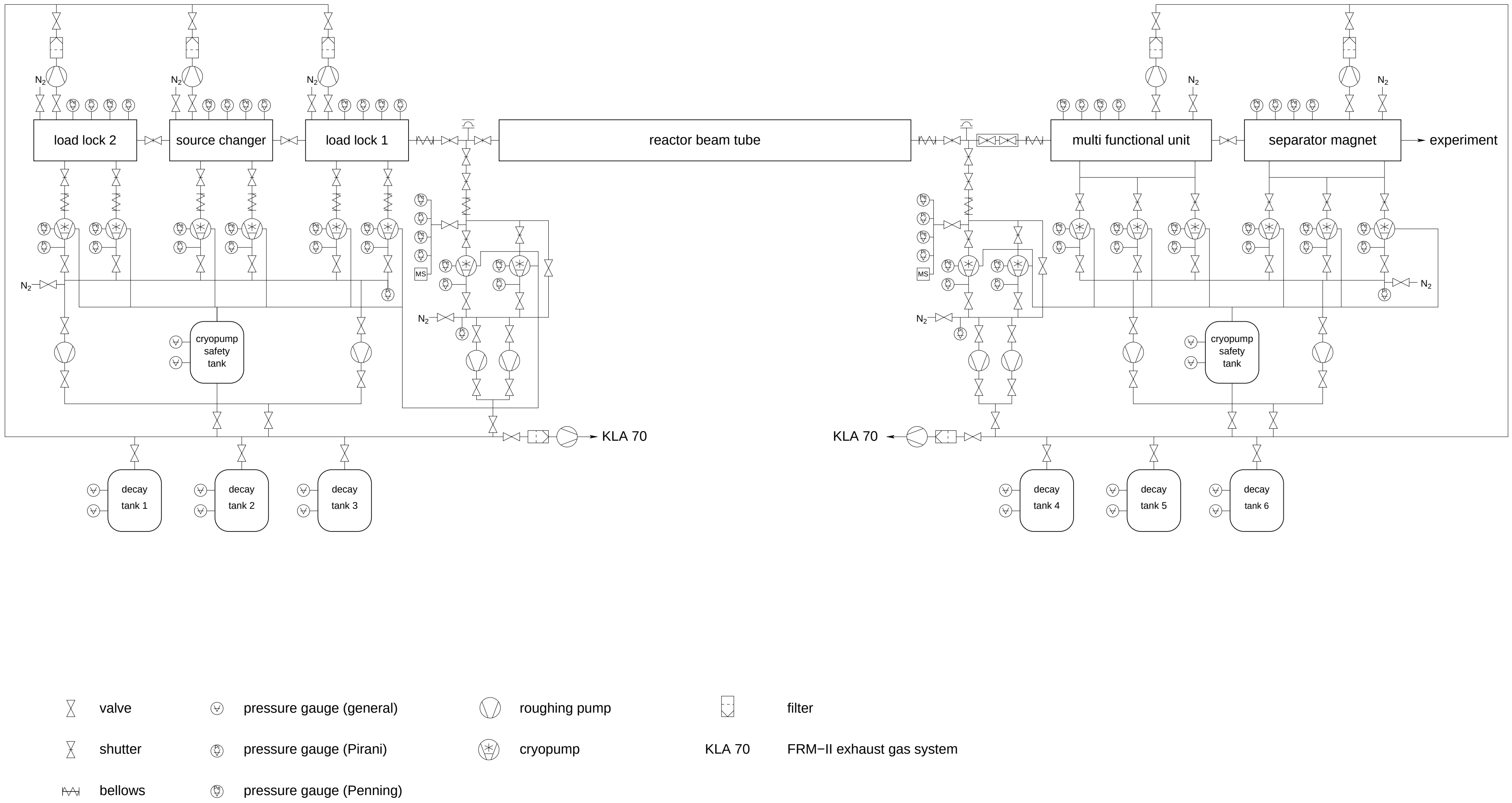

Fig. 6: Schematic view of the MAFF vacuum system

During regeneration the formation of aerosols is not likely, because the solid daughters of the noble gases are formed where the Kr and Xe atoms are adsorbed to the charcoal of the second stage (10 K) of the cryopump, whereas the dominant partial pressure which origin is outgassing is water, and this is bound on the first stage of the cryopump at a temperature of about 70 K. During warm-up of the cryopump for regeneration firstly Kr and Xe are released from the second stage, due to their noble gas character they can not bound solid fission products to be transported with them. When finally the first stage is warmed up and huge amounts of water vapor are released, they can not carry fission products, because on the first stage no Kr or Xe were bound. Therefore solid fission products could only be released from the cryopump by second order effects. This means that most of the radioactive inventory is stored in the cryopumps and will not be carried off into the decay tanks or in a second step into KLA 70.

Such cryopumps are well suited for storing radioactivity. The critical parts in vacuum are the charcoal covered condensation surfaces. The charcoal is bound by an organic two component adhesive to the copper panels. This was tested at CERN, where a stability of 10^7 Gy was approved and this not only statically but in addition with a static-vibration test. There are no moving parts in the vacuum container of the cryopump. The cold head is metallically sealed to the pump vessel. Their displacers and the pressurized He gas supply withstands only irradiation of 10^4 Gy, but these parts can be exchanged in routine service intervals without braking the vacuum, they are not contaminated.

Filling of the decay tanks is only allowed to a pressure of about 900 hPa to guarantee that in case of a leakage no radioactivity will be released. The underpressure in combination with no circulation of the gas help the decay of aerosols, thus aerosol-bound solid fission products might stick to the tank walls after release from their gas partners. Slowly evacuating the decay tank for discharging into KLA 70 should prevent that major parts of the wall bound fission products would be removed. Oil lubricated rotary vane pumps are not well suited as roughing pumps for this application. It is planned to install the EcoDry M pumps from LEYBOLD. Unfortunately such dry pumps have a Helium leak rate of $0.01\ \mathrm{Pa} \cdot \mathrm{l} \cdot \mathrm{s}^{-1}$ which is, however, not a real problem, because inlet and exhaust ports are always below atmosphere pressure. Thus no radioactivity can leak through these pumps. There are two main reasons why only dry pumps can be applied. During regeneration of a cryopump the roughing pump works at its ultimate vacuum, thus backstreaming is the normal case. Oil vapors would condense on both stages of the cryopump as long as the pump is not completely warmed up. The pumping surfaces of the charcoal would be covered thus dramatically reducing their pumping speed and capacity. The second reason is that rotary vane pumps generate oil mist at their exhaust which could clog the aerosol filters.

In case of a longer electricity shut down, the cryopumps will warm up and release their bound gases. If thus the pressure in a cryopump exceeds 1500 hPa a rupture disk is destroyed and the gas is discharged into a safety tank which was evacuated before to $< 100\ Pa$.

3.3 Beam extraction and mass separation

The concept of the mass separator is adopted to the double-humped mass distribution of fission fragments. It is planned to transmit one beam of ions from either mass group. The average masses of the heavy and the light group have a ratio of 3:2. Their magnetic rigidities thus have a ratio of 1.22 and the separator magnet has to have a corresponding exit width. Both beams then are injected into cooling sections which reduce the transversal beam emittance and pulse the beam into short packets. Special care had to be taken in the design of the isotope separator, because only a small sector of space is available.

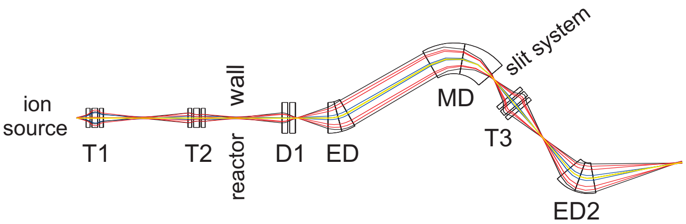

Fig. 7: Beam transport from the ion source out of the reactor and mass separation. Elements of the beam optics are quadrupole triplets (T) and doublet (D) as well as electric (ED) and magnetic deflectors (MD).

After extraction of the ions with an electrode at ground potential, the 30 keV ions are transported out of the reactor vessel. Calculated ion beam trajectories (code: COSY INFINITY [6]) in the horizontal plane are shown in Fig. 7 for one mass only (A=139). In order to accommodate neutron and gamma absorbers, the beam is focused with two electrostatic quadrupole triplets (T1,T2) and one doublet(D1), producing a waist between either pair of lenses.

In every lense system one quadrupole is provided with four voltages. That allows steering in both transverse dimensions.

For the mass separation we use a modified version of a Mattauch-Herzog configuration [7] with a 30° electrostatic deflection (ED, $r = 1\ m$) and an 80° magnetic deflection (MD, $r = 1.24\ m$ for A=139). The reduction of the latter deflection angle from the ideal 90° results in a focal plane 230 mm behind the edge of the pole piece. At this position nearly all radioactive ions are dumped on the slit system and just two masses are transmitted further.

The Mattauch-Herzog configuration has the advantage that the total deflection is independent of energy to first order. Thus small changes of the ion source potential do not destroy the mass separation.

In front of the separator we use a doublet to produce the object focus in the horizontal plane and in the vertical plane the trajectories are made to cross inside the MD thus allowing for a small gap of the magnet.

We chose the ED as first deflection, because it can easily be removed to allow access to the through-going beam tube and because the magnet is not in line of sight of the reactor neutrons and thus activation of material is reduced. However, in order to view the ion source and the extraction electrode from the outside and to be able to irradiate (in a later stage) the ion source with laser light for resonant ionization, the positive electrode of the ED has to have a bore in the direction of the beam tube. With a mirror behind the deflector light can be inflected onto the beam axis. After that we will place shielding material to absorb neutrons and gammas.

The mass dispersion at the focus behind the MD is about 5 mm/% and the horizontal magnification is 2.6 from the "focus" at the ion source. The trajectories in Fig. 7 have been calculated for a beam emittance of $\pi \cdot 1mm \cdot 30mrad$ leading to a mass resolution of about 190. As described above, calculated emittances for the ion source are nearly an order of magnitude smaller and already in first tests with a prototype a factor of two better emittance at 20 keV was observed [8]. Thus the mass resolution will be accordingly better. With the slit system at the focal plane two masses will be selected and transmitted, while the dominant fraction of the radioactive ions are dumped on the slits. The transmitted beams will be refocussed and electrostatically deflected towards the beam cooling sections.

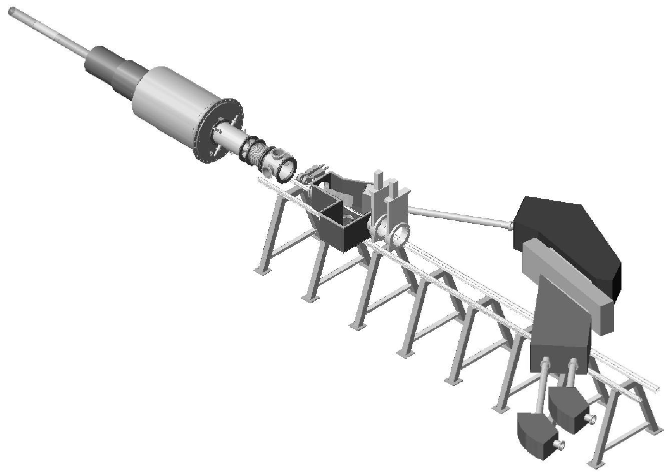

Fig. 8: Sketch of the main components for beam extraction and mass separation. The tube on the left side houses the extraction electrode and the lenses. It is inserted through an outer and inner shielding plug, in which it is moved by a carriage. After a section with electrical and helium feedthroughs and the valves forming the barriers to contain the radioactivity, there is a multi-purpose unit containing the electrostatic deflector (removable), shielding material and an optical mirror. The magnetic deflector, the chamber for the slit system, a box housing the lenses, and the final deflectors are also visible.

The carriage with extraction electrode and lenses has to move through the shielding plug. Therefore the presently mounted solid shielding plug has to be replaced. The inside has to be provided with an elaborate mechanical construction for the movement and the precise positioning of the lense carriage. Since the details of this construction will only be finalized at a later date, we intend to use an outer and an inner plug.

In Fig. 8 only the outer plug is visible protruding further towards the reactore core. With an outer diameter of 870 mm it will have most of the weight but has to be mounted only once. The inner plug with an outer diameter of 520 mm rests in the outer one, which has little mechanical details. Until the final inner plug is constructed and mounted, we will close the opening in the outer one by a provisional solid inner plug.

As already mentioned, the ED and the shielding behind it have also to be removed, when the lense carriage is moved out. This happens in the multi-functional unit (MFU), which also houses the optical mirror system behind the ED. For the removal of the lense carriage a shielding bottle can be attached to the end of the MFU, into which the carriage is moved under vacuum.

In order to study the manufacturing of the quadrupole lenses with materials, that can sustain high temperatures, we have constructed and built a quadrupole triplet from MACOR and aluminum (Fig. 9). The aluminum will be replaced by titanium in the final version. In addition we had to save as much weight as possible, since the tube in which the lenses are mounted, should not bend more than a few mm. The lense with a full aperture of 50 mm will be tested at the MLL ion source test bench.

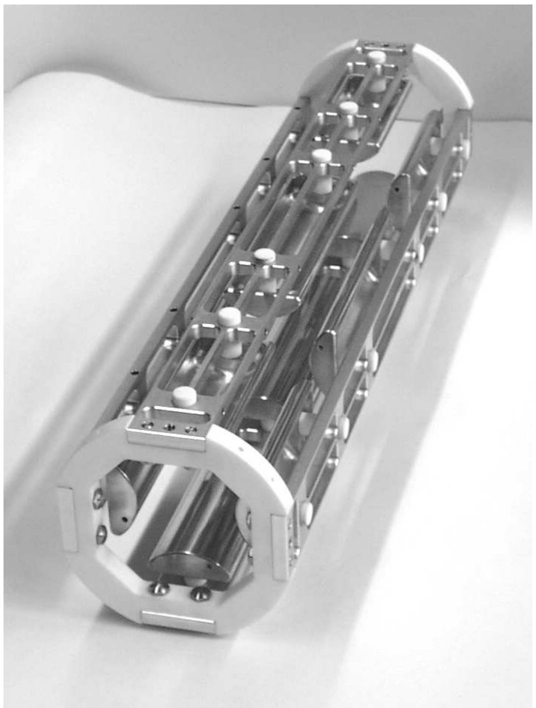

Fig. 9: Quadrupole triplet 450mm long, 50mm aperture.

3.4 Design Status for the MAFF-RFQ

For the MAFF-Linac [11] the first acceleration stage consist in an IH-RFQ operating at 101.28 MHz frequency and at maximum duty cycle of 10%. The MAFF IH-RFQ will accelerate ions with $A/q < 6.5$ from 2.5 keV injection energy to about 300 keV/u. Simulation of the electromagnetic properties of the resonator has been performed with `MAFIA` and `MWS` [12] and an optimized geometry has been proposed in [13]. The calculation performed with the code `MWS` has shown significant differences in the shunt impedance and in the power dissipation with respect to `MAFIA`. The differences are due to the different meshing procedure for a given boundary condition and the accuracy of the results depends a lot on the simulation technique [14].

The construction of a prototype short model in aluminum has been proposed as a benchmark of the calculation and it will be used for frequency and voltage-flatness measurement and to test the tuning procedure of the cavity. This test will allow to set the final geometry for the real resonator.

The latest calculations are summarized in table 1.

Frequency f	102.64 MHz
Q-value	7932
Shunt Impedance R_p	196 kΩm
Flatness of the ref voltage	< 1.5%
Vertical dipole component α	< 1.5%
Power on the electrodes	12.1%
Power on the stems	36.8 %

Table 1: RF parameters and power distribution of the IH-RFQ

The mechanical construction of the resonator plays a major role in this kind of structure since the high efficiency, in term of R_p values, can be maintained only if the number of brazing and welding procedure is limited. For assembly reason the 3 m long resonator has been splitted in 4 identical modules plus 2 end parts which contains the undercut regions. This longitudinal splitting does not compromise the electrical properties of the resonator since the current flow is mainly in the transverse plane as fig. 11 shows.

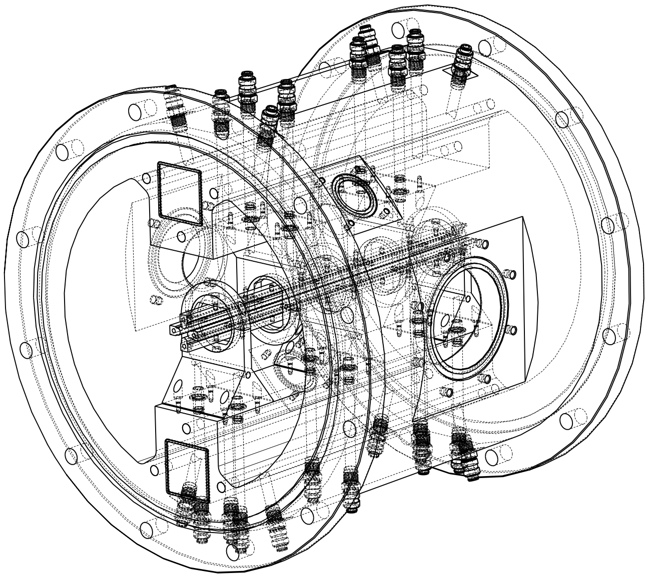

Fig. 10: Mechanical drawing of one of the central modules of the MAFF IH-RFQ (length: 40 cm, inner diameter: 310 mm).

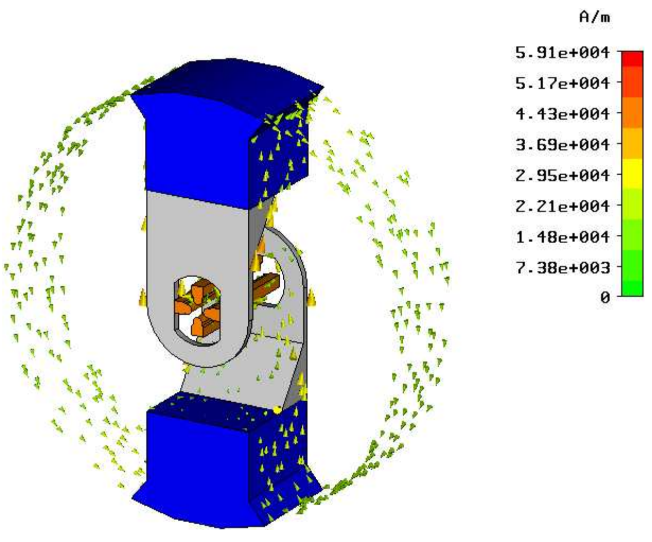

Fig. 11: Surface current in the single cell model of MAFF IH-RFQ

From the manifacturing point of view, each module will be carved via wire erosion from a massive copper cylinder to preserve the electrical conductivity. The choice of building the whole structure from copper is required because we want to keep the thermal conductunce as high as possible since the electrodes are only indirectly cooled.

On the particle dynamics side, the electrode design of the MAFF-RFQ could be derived by PARMTEQ calculations from the design of the comparable REX-RFQ [15]. The input energy is 2.5 keV/u, the final energy 300 keV/u at a length of 3 m (287 acceleration cells). The design could be optimized to a transmission higher than 99%, while the energy and phase spread are $\pm$1.5% and $\pm$15 degrees. The radial acceptance is 200 π mm mrad. Figure 12 shows the electrode Parameters of the MAFF-RFQ at one glance. Calculation with high order in the potential funtion will be performed as a final review of the beam dynamics.

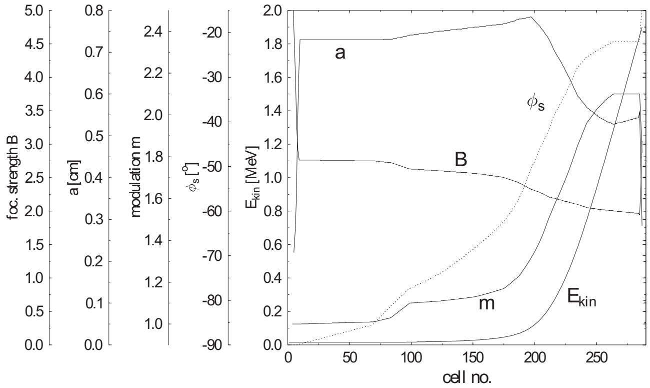

Fig. 12: Electrode design of the MAFF-RFQ, calculated with PARMTEQ. Plotted is the radial focusing strength (B), the aperture (a), the modulation (m), the synchronous phase (ϕ) and the particle energy (E).

3.5 The IH-7-gap Structure Prototype

The key element of the energy variable part of the MAFF-LINAC are the IH-7-gap resonators, which allow to vary the beam energy for experiments. In order to cover the entire range of 3.7-5.9 MeV/u two of those structures are required. In order to examine the properties of that ion accelerator cavity, a prototype has been developped [16]. The IH-7-gap resonator will be operated at 202.56 MHz resonance frequency an can be driven with a maximum duty cycle of 10%.

In 2002 the final dimensions of the IH-7-Gap resonator were determined by measurements taken at the manufacturer (NTG) in February 2002 [17]. The proposed changes of the flanges of the half shells for frequency tuning were carried out and the tank was copper plated at GSI afterwards. After the copper plating, the resonator was transported to Munich and low level measurements, both for the 7-Gap and the 9-Gap configuration relevant for REX-ISOLDE, were carried out to verify that the resonator characteristics of the finished tank agree to the calculations. These low level measurements consisted of resonance spectra, quality factors, shuntimpedances and gap voltage distributions. The results were in good agreement with the estimations from other IH-structures, but differ as known from MAFIA calculations. Due to the high quality factor after copper plating the resonance frequencies were slightly higher (approximatly 0.4 MHz) than expected but still in the acceptable tolerance range. The spectra showed no mode mixing between 150 MHz and 300 MHz. The quality factors of the resonator are 9833 (7-Gap) and 10100 (9-Gap) respectively. These values are approxmatly 30% lower than the MAFIA calculations of 15000. This was expected, based on experiences with similar structures [18]. Shuntimpedances and gap voltage distributions were determined by bead-pull measurements. The values of the shuntimpedances correspond to the values of the quality factors (table 2).

	Quality Factor Q_0	**Shuntimpedance** Z
MAFIA 7-Gap	15000	180 MΩ/m
MAFIA 9-Gap	15500	300 MΩ/m
Modell 7-Gap	max. 3800	max 46 MΩ/m
Power resonator 7-Gap	9833	140 ± 12 MΩ/m
Power resonator 9-Gap	10100	202 ± 13 MΩ/m

Table 2: Comparison between the proposed (MAFIA 4.0) and measured values of the quality factors and shuntimpedances.

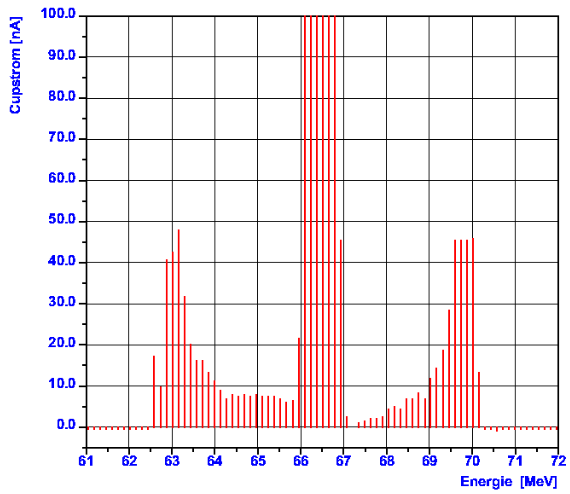

Fig. 13: Energy modulated DC beam at 12 kW amplifier power.

A test bench for high power measurements was set up at the -25^o beam line of the MLL. It was possible to obtain momentum spectra of a DC beam at different amplifier powers (figure 13) and spectra for beam pulses at different phases 14, using a 70^o bending magnet positioned behind the resonator tank. The energy modulation spectra with a dc-beam from the tandem were used to determine the effective shunt impedance. The measurement with pulsed beam injected into the 7-gap structures have been done to determine the possibility to vary the beam energy by tuning the resonator phase and amplitude. Since the tandem can not deliver ions with $A/q = 6.3$ and an energy of 4.15 MeV/u or 5.40 Mev/u respectivly, a 66.4 MeV $^{16}O^{5+}$ beam was used and due to the $A/q = 3.2$ the power was reduced by a factor of 3.9. This way, the worst case scenario of deceleration and acceleration from 4.15 MeV/u could be examined. The power amplifier used to perform the high level tests had a duty cycle of only 1:500 (1 ms pulse at 2 Hz) and the repetition rate of the amplifier mismatched the repetion rate of the low energy chopper of the tandem. Therefore the spectra show a non-accelerated component of the beam from the tandem that could be used to calibrate the measurements.

In the spectra of the DC beam all phases to the synchronous particle are repesented. Therefore the primary beam from the tandem is modulated in dependence of the applied HF-power. This results in a continous spectrum between the maximum decelerated and maximum accelerated particles (phase = 180^o or 0^o respectivly to the synchronous particle). In the pulsed mode every 40th bucket contains a particle bunch. By shifting the phase between the power amplifier of the resonator and amplifier of the buncher the phase of the bunch to the synchronous particle could be adjusted. The measurements have shown that the required energy range can be covered with 20 kW rf-power, which correspond to approx. 80 kW for particles with $A/q = 6.3$.

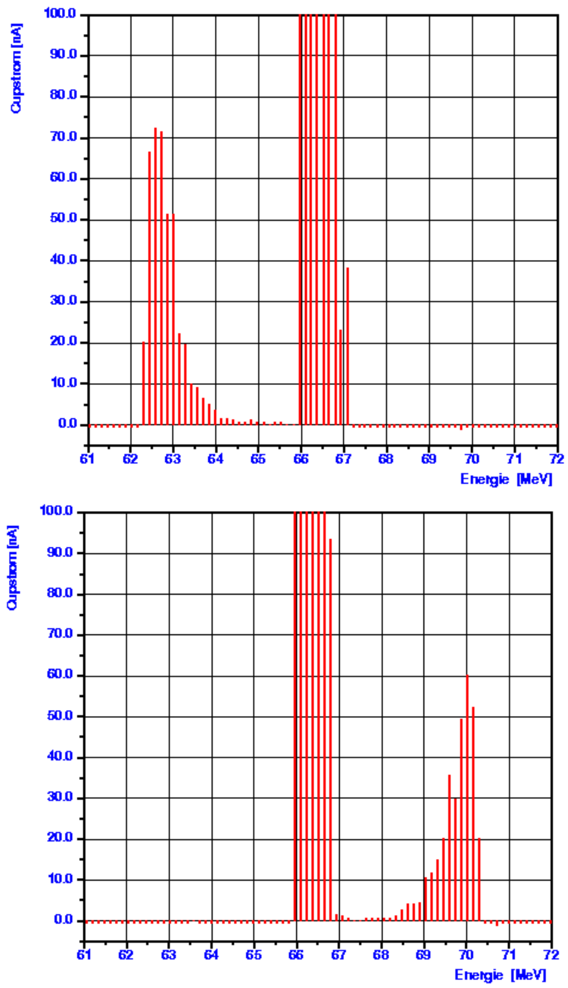

Fig. 14: Acceleration and deceleration for pulsed beams at 15 kW power.

By analysing these spectra it was possible to determine the effektive shuntimpedances of the resonator for acceleration and deceleratio at different power levels and calculate the total shuntimpedance (figure 17) by using simulation calculations. The dependency of the effective shuntimpedance on the amplifier power is distinctivly different for acceleration and deceleration. Since the beam is injected with an energy significantly below the design energy the transit-time factor changes in dependence on the power. While for deceleration the transit time factor of the resonator (and therefore the effective shuntimpedance) decreases with increased power, for acceleration the transit-time factor increases, which can be seen in figures 15 16. Moreover, due to various thermal effects a general drop of the total shuntimpedance is expected at higher power levels [19], which becomes obvious in figure 17.

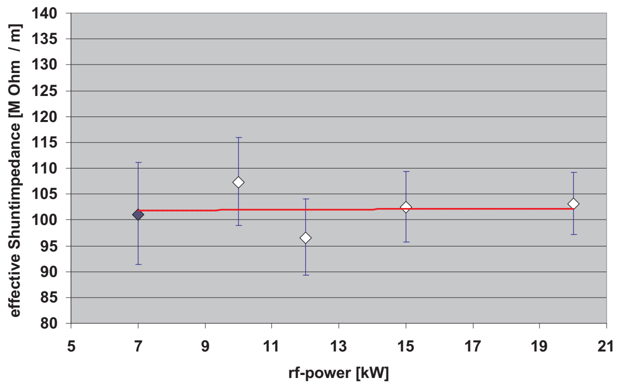

Fig. 15: Shunt impedance for acceleration in dependence of the amplifier power.

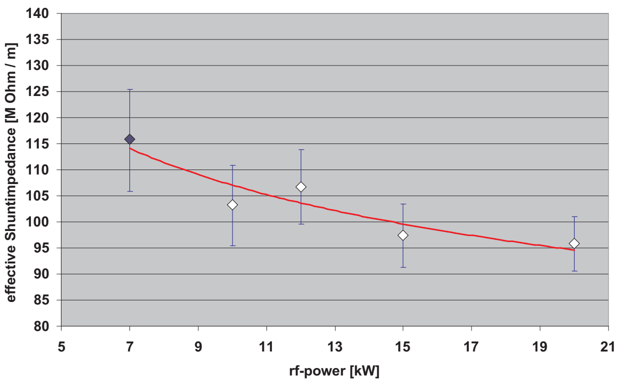

Fig. 16: Shunt impedance for deceleration in dependence of the amplifier power.

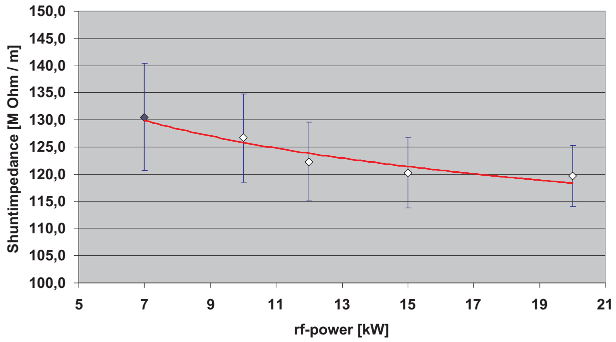

Fig. 17: Total shunt impedance in dependence of the amplifier power.

To reach the proposed energy gain of 0.32 MeV/u per resonator, necessary to obtain an overlap in the final energies for both injection energies (4.15 MeV/u and 5.4 MeV/u), an effective shuntimpedance of at least 82 MΩ/m is mandatory for acceleration [17]. Figure 15 shows, that the effective shuntimpedance for deceleration decreases with increasing power, while the effective shuntimpedance for acceleration stays stable at approximatly 102 MΩ/m over the entire power range available on the test beam line (figure 16).

References

[1] *MAFF — Physics Case and Technical Description,* ed. by D. Habs *et al.*, `http://www.ha.physik.uni-muenchen.de/maff/`

[2] D. Habs *et al.*, *The Munich Accelerator for Fission Fragments MAFF,* Proc. EMIS-14, to be published in NIM B

[3] H. Bongers *et al.* Rev. Sci. Instrum. **73** (2002) 809

[4] H.-J. Maier *et al.* Annual report 2001, p. 80

[5] F. Ospald F. Ospald, diploma thesis, LMU München, 2002

[6] K. Makino, M. Berz; Nucl. Inst. Meth. **A427** (1999) 338

[7] J. Mattauch, R. Herzog; Z. Physik **89** (1934) 786

[8] F. Ospald, diploma thesis, LMU München, 2002

[9] Technical report of the PIAFE project, ISN 97-52

[10] M. Guisset, J. L. Bouly, Pompagne des gaz radioactifs dans les zones 1 et 2, ISNGPIAFE/Np/1009, 1996

[11] O. Kester *et al.*, The Munich Accelerator for Fission Fragments (MAFF), AIP Conf. Proc. **473** (1998) 536

[12] CST Computer Simulation Technology http://www.cst-world.com

[13] T. Sieber, Ph.D. thesis, LMU München, 2001

[14] M. Pasini, Notes on MAFF IH-RFQ simulation with `MWS`

[15] T. Sieber *et al.*, Design and Status of the RFQ for REX-ISOLDE, Proc. LINAC'98, Chicago (1998) 777

[16] H. Bongers, Ph.D. thesis, LMU München, 2002

[17] H. Bongers *et al.* Annual report 2001, p. 73

[18] S. Emhofer, diploma thesis, LMU München, 1999

[19] H. Podlech, Dissertation, Universität Heidelberg, 1999